Asian Journal of Chemistry; Vol. 38, No. 6 (2026), 1556-1564
ASIAN JOURNAL OF CHEMISTRY
https://doi.org/10.14233/ajchem.2026.36002

Effect of Substituents at α- and β-Carbon Atoms on β-Elimination Reactions of *N*-Alkyl Pyrazoles: A Theoretical Approach

SANJEEV KUMAR MISHRA and JYOTI TYAGI*

Department of Chemistry, Zakir Husain Delhi College, University of Delhi, New Delhi-110002, India

*Corresponding author: E-mail: jyoti.tyagi@zh.du.ac.in

Received: 2 March 2026 *Accepted*: 2 May 2026 *Published online*: 31 May 2026 AJC-22382

The present study investigates the effect of substituents at the α- and β-carbon atoms on the β-elimination reactions of N-alkyl pyrazoles using density functional theory (DFT). Five elimination pathways involving different substituent combinations, namely hydrogen, methyl and ethyl groups, were examined in detail to evaluate their influence on reaction energetics and transition-state characteristics. *N*-Ethyl pyrazole, *N*-*sec*-butyl pyrazole, *N*-*tert*-butyl pyrazole and *N*-*tert*-pentyl pyrazole were selected as model reactants, which upon β-elimination yielded the corresponding alkene along with pyrazole as the common product. The variations in ΔH values are observed among the five reactions. Substitution with all methyl group has significant effect on activation energy and energy of reaction. Interestingly, this study reveals that methyl and ethyl group have negative inductive effect on α- and β-carbon atoms. The results obtained in this work align well with the previous reported experimental kinetic study and demonstrates improved accuracy as compared to semi-empirical study. Moreover, this study sheds light on the mechanistic aspects of β-elimination reactions of *N*-alkyl pyrazoles and enhances academic knowledge on the effect of methyl and ethyl group in organic molecules.

Keywords: Alkene, Pyrazole, Transition state, Hofmann reaction, Mechanism, DFT, Intrinsic reaction coordinate.

INTRODUCTION

Pyrazoles are five-membered aromatic heterocycles containing two adjacent nitrogen atoms and are recognized for their wide range of biological activities [1]. Pyrazole derivatives exhibit diverse pharmacological properties including antiviral, anticancer, antimicrobial, anti-inflammatory and antipyretic activities [2,3]. Due to these therapeutic applications, pyrazole scaffolds are frequently incorporated into biologically active molecules and pharmaceutical compounds. In addition to their medicinal importance, *N*-alkyl pyrazoles serve as useful synthetic intermediates for the incorporation of pyrazole moieties into structurally complex molecules. These derivatives also possess considerable industrial relevance and are widely employed in agrochemical formulations such as pesticides, insecticides and herbicides [4]. Furthermore, substituted pyrazoles have gained increasing attention in material science due to their potential applications in batteries, energetic materials and chemical sensors [5-8].

N-Alkyl substituted pyrazoles undergo β-elimination reactions to produce pyrazole and the corresponding olefinic products. These reactions are generally base-catalysed and may proceed through either E1 or E2 mechanisms depending on the reaction conditions and the nature of the alkyl substituent [9]. In the presence of a base, *N*-alkyl pyrazoles predominantly undergo Hofmann-type β-elimination through an E2 pathway. Under gas-phase thermal conditions, these compounds also yield pyrazole and alkene products *via* a concerted E2 elimination process. Kinetic studies have demonstrated that the reaction proceeds through a five-membered cyclic transition state leading to the formation of pyrazole and olefins [10]. The elimination follows the Hoffmann rule, favouring the formation of the least substituted alkene. Consequently, this process provides a useful route for the synthesis of small and light olefins from *N*-alkyl pyrazoles.

Gas-phase elimination reactions of *N*-alkyl pyrazoles have also been investigated using semi-empirical theoretical methods to gain insight into the reaction mechanism. Theoretical studies suggested a concerted unimolecular pathway involving a five-membered cyclic transition state [11]. The calculated activation energies were found to be relatively higher, approximately 25 kcal mol^{-1}, compared with the experimental kinetic

values. Nevertheless, the substituent-dependent variations in activation energies showed good agreement with the experimental observations.

Although experimental and semi-empirical studies on the gas-phase β-elimination reactions of *N*-alkyl pyrazoles have been reported, higher-level theoretical calculations are still limited. Moreover, discrepancies between experimental activation energies and semi-empirical predictions remain unresolved. To address this gap, the present study employs density functional theory (DFT) to investigate the thermal β-elimination reactions of *N*-alkyl pyrazoles bearing different substituents at the α- and β-carbon positions. The investigated gas-phase reactions proceed to form pyrazole along with the corresponding olefinic products. The study is expected to improve the understanding of substituent effects and mechanistic aspects associated with β-elimination reactions.

EXPERIMENTAL

In the present work, the DFT calculations were performed at the B3LYP/6-311++G(d,p) level. Geometries of all the reactants (*N*-alkyl pyrazoles), products (pyrazole and alkene) and transition states (TS1, TS2, TS3, TS4 and TS5) were optimised using the aforementioned method [12-14]. Five elimination reactions were studied in detail and their corresponding TS structures were also determined. To have the better understanding of the reaction mechanism of the elimination reactions, electronic charge density (ρ_c) and Laplacian density ($\nabla^2\rho_c$), which are known as bonding characteristics were calculated [15]. For all the structures under study, harmonic vibrational frequencies (scaled down by a factor of 0.968) were determined to identify the stationary points of a particular geometry [16]. Energetics of the elimination reactions were studied *via* calculating activation energy and enthalpy of reaction at the same level of calculation that has been used for geometry optimisation. Entropy and free energy of the reaction were also calculated at 298.15 K. Reaction paths for all the five reactions were investigated through intrinsic reaction coordinate at the same basis set. Also, natural atomic charges on different atoms were also calculated using NBO analysis to understand the transfer of charges during the elimination reaction [17-19].

RESULTS AND DISCUSSION

Structures of reactants, transition states and products: In present theoretical DFT study, β-elimination reaction of *N*-alkyl pyrazoles is studied in detail for five *N*-alkyl pyrazoles as shown in Fig. 1. Geometry of the five reactants, *viz. N*-ethyl pyrazole (**1**), *N-sec*-butyl pyrazole (**4a** and **4b**), *N-tert*-butyl pyrazole (**7**) and *N-tert*-pentyl pyrazole (**9**) were optimised using B3LYP/6-311++G(d,p) method. All the products formed in the five elimination reactions, *viz.* pyrazole (**2**), ethene (**3**), but-2-ene (**5**), but-1-ene (**6**), 2-methylpropene (**8**) and 2-methyl-but-2-ene (**10**) were also fully geometrically optimised at the same level. The optimised transition states, *viz.* TS1, TS2, TS3, TS4 and TS5 formed in the five considered elimination reactions (reaction I to V) are shown in Fig. 2. The geometric parameters (bond lengths, bond angles and dihedral angles) for all the structures of reactants, products and transition states that are obtained after calculations are tabulated in the Tables 1 and 2.

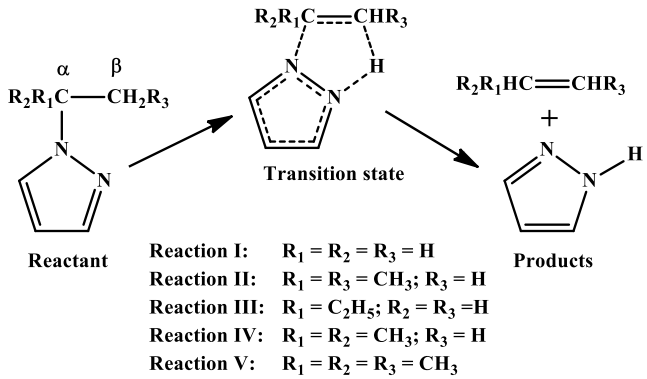

Fig. 1. β-Elimination reaction mechanism in N-alkyl pyrazoles

Formation of pyrazole and ethene (reaction I): In reaction I, *N*-ethyl pyrazole (**1**) converts to pyrazole (**2**) and ethene (**3**) *via* TS1 as shown in Fig. 2. There is a significant increase in the N2-C3 bond length from 1.459 Å to 2.002 Å during the transition of **1** to TS1, which is also supported by a decrease in the electronic charge density to 0.076 (TS1) from

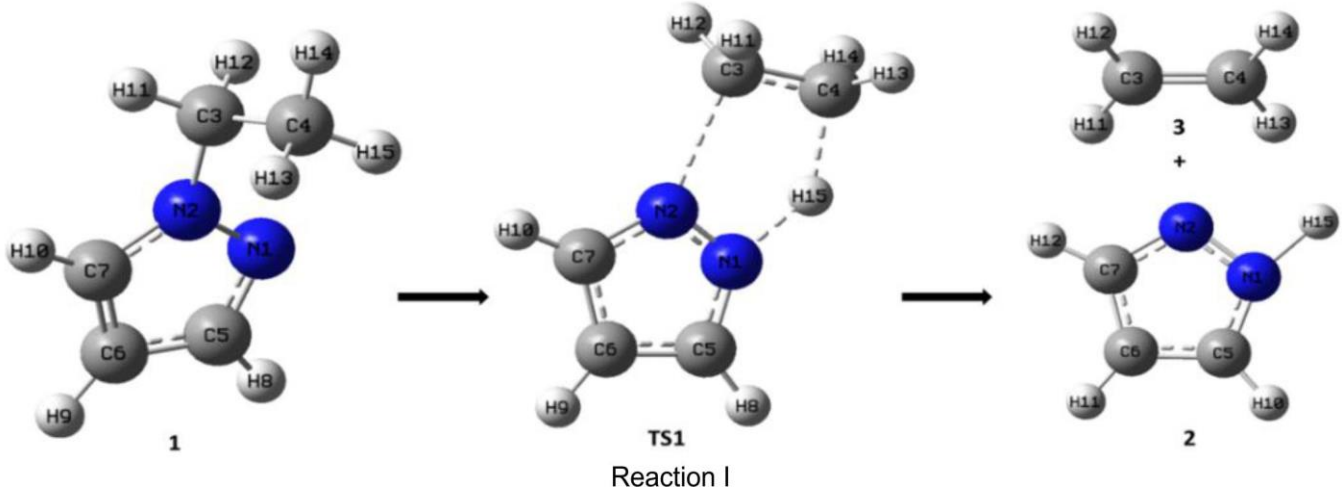

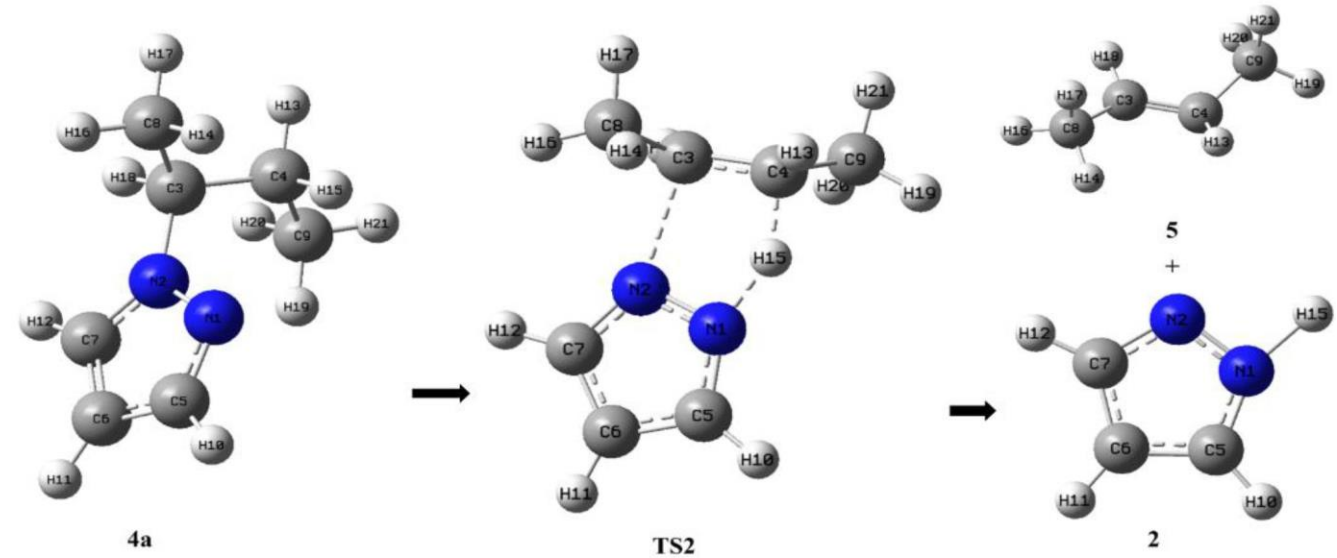

Reaction II

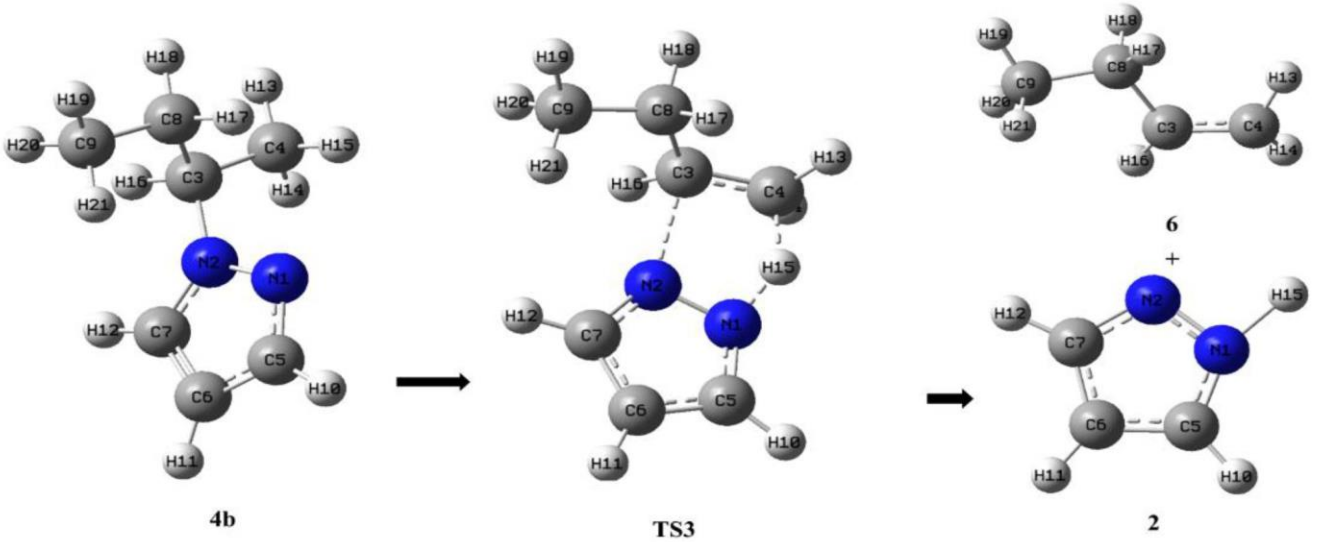

Reaction III

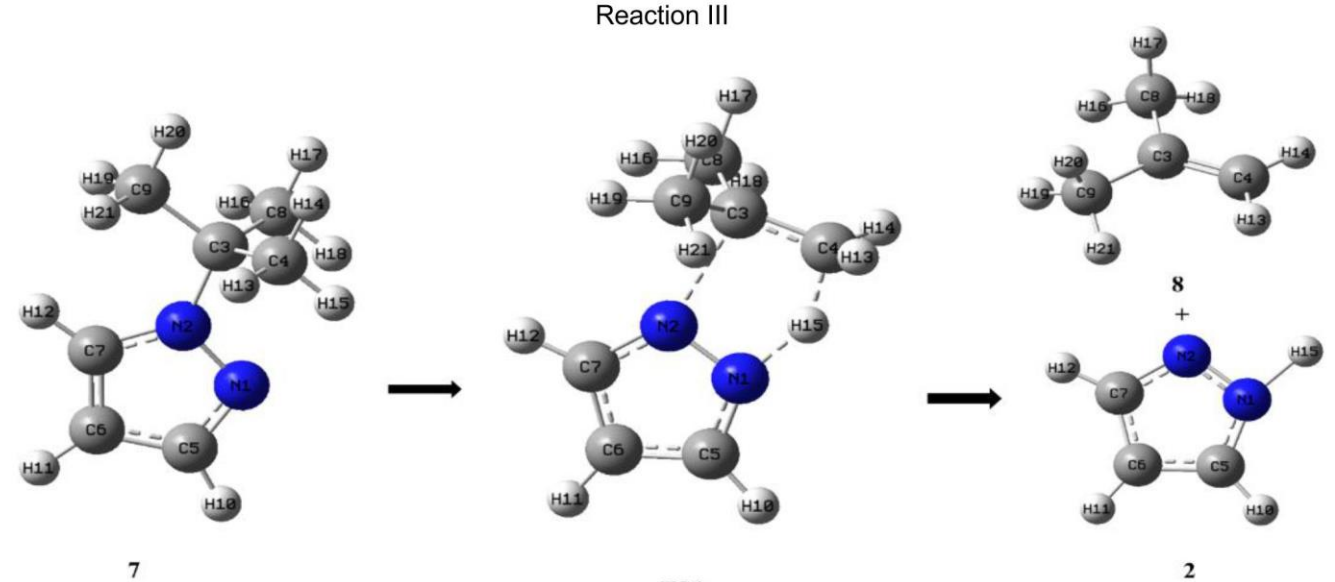

Reaction IV

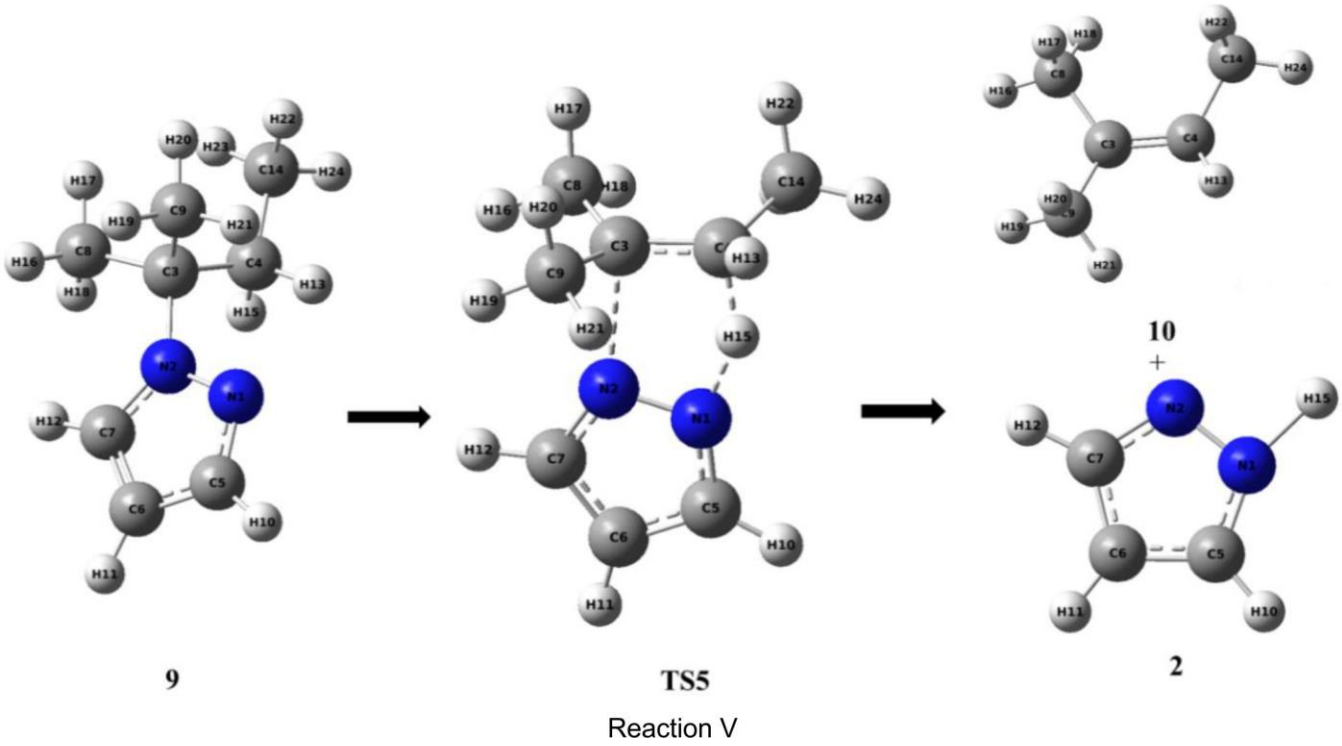

Fig. 2. Optimised geometry of reactants, transition states and products for reactions I-V

0.257 (**1**). The bond C4-H15 elongates to 1.425 Å in TS1 from 1.091 Å in **1** along with a decrease in $\rho(r_c)$ value in TS1, supporting the weakening of the bond. Atom N1 and H15 come closer to each other in the TS1 as the distance between the two is 1.279 Å and $\rho(r_c)$ value for the same is found to be 0.162 with a negative value (-0.021) of Laplacian density showing the non-ionic interaction between the two. The bond between C3-C4 gets shorten in TS1 showing the development of the double bond character. It is interesting to note that N1-N2 bond becomes slightly stronger in TS1 as supported by an increase in $\rho(r_c)$ value and decrease in $\nabla^2\rho_c$ value (Table-2). The bond angle N1-N2-C3, N2-C3-C4 and C3-C4-H15 decreases while transition of reactant (**1**) to TS1. Also, the angle N1-H15-C4 and N2-N1-H15 are observed to be 142.4º and 99.6º in TS1. The magnitude of dihedral angles shows the planarity of the TS1. All these changes in geometric parameters supports the formation of a five-membered planar cyclic transition state TS1. In our calculations, exactly one imaginary vibrational frequency for TS1 with high magnitude as well as high intensity (Table-3) is observed that validates an acceptable TS structure of first-order. This negative frequency corresponds to stretching mode indicating shifting of H15 to N3 atom. The IRC plot for the reaction I is shown in Fig. 3. Also, the all-positive values of frequencies for reactant (**1**) and product (**2** and **3**) indicates the stable geometries. Natural atomic charges calculated *via* NBO analysis are tabulated in Table-4. Charge on atom C3 becomes less negative and that on H15 increases to 0.379 as **1** change to TS1, which is also supporting the fact of C3 going away and H15 coming closer to N1. The negative charge on C4 atom increases during the transition of **1** to TS1 that further supports the proton transfer from alkyl group to N of pyrazole ring.

Formation of pyrazole, but-2-ene and but-1-ene (reaction II and III): In reaction II, N-*sec*-butyl pyrazole (**4a**) converts to pyrazole (**2**) and but-2-ene (**5**) *via* TS2 while in reaction III, N-*sec*-butyl pyrazole (**4b**) yields pyrazole (**2**) and but-1-ene (**6**) thru TS3. In these two reactions, starting reactant is same but the product olefin found to be existed in two structural isomers, *viz.* but-2-ene and but-1-ene. In these two reactions, N2-C3 and C4-H15 bond elongates (Table-1) during the transition of **4a** and **4b** to TS2 and TS3, similar to reaction I. Furthermore, the magnitude of $\beta(r_c)$ for the two bonds also supports the bond lengthening (Table-2). In these two reactions, changes in the others structural parameters follow the same pattern, *i.e.*, shortening of C3-C4 and N1-N2 bond and close proximity of N1 and H15 atom. The changes in angles and dihedral angles are also found to be similar to that in reaction I. The value of electronic charge density and Laplacian density also supports the changes in the structural parameters (Table-2). The TS structure in reaction II and III, *viz.*, TS2 and TS3 also possess single negative frequency with high magnitude and intensity indicating a valid TS. The vibrational frequency analysis of the reactants and products formed in these reactions (II & III) suggests the stable geometry of all (Table-3). The IRC plot of these two reactions is presented in Fig. 3. Examination of the natural atomic charges on the C3 and C4 atoms in 4a clearly reveals the influence of methyl group substitution on the electronic distribution around these carbon centres. The negative charge decreases on both the atoms by an approximately same magnitude showing the electron withdrawing nature of an alkyl group. Furthermore, the charge in **4b** on the atom C3, also reveals the same effect of an ethyl group (-I) on C3 atom. Since C4 is not substituted in **4b**, the charge is of the same magnitude as that on C4 atom

TABLE-1
SELECTED GEOMETRIC PARAMETERS USING B3LYP/6-311++G(d,p)

System	**1**	TS1	**2**	**3**	**4a**	TS2	**5**	**4b**
Lengths (Å)								
N1-N2	1.348	1.313	1.348	–	1.348	1.316	–	1.410
N2-C3	1.459	2.002	–	–	1.471	2.125	–	1.470
C3-C4	1.528	1.405	–	1.329	1.531	1.407	1.333	1.540
C4-H15	1.091	1.425	–	–	1.092	1.341	–	1.070
N1-H15	–	1.279	1.007	–	–	1.348	–	2.650
C4-H13	1.093	1.086	–	1.0851	1.092	1.092	1.090	1.070
N1-C5	1.332	1.345	1.358	–	1.332	1.346	–	1.304
N2-C7	1.358	1.340	1.329	–	1.358	1.342	–	1.334
Angles (º)								
N1-N2-C3	119.8	102.4	–	–	120.2	100.6	–	125.3
N2-C3-C4	112.8	101.3	–	–	110.9	98.5	–	109.5
N1-H15-C4	–	142.4	–	–	–	147.4	–	-
C3-C4-H15	110.4	94.3	–	–	110.3	95.2	–	109.5
N2-N1-H15	-	99.6	119.0	–	–	97.6	–	–
C3-N2-C7	128.1	148.4	-	–	127.8	150.5	–	125.3
N1-C5-H10	120.7	121.3	122.0	–	119.6	121.3	–	125.2
C3-C4-H13	111.1	117.7	–	121.7	110.2	114.7	118.6	109.5
Dihedral angles (º)								
N1-H15-C4-H13	–	119.8	–	–	–	127.7	–	–
N1-N2-C3-C4	-72.0	-0.018	–	–	-64.7	5.6	–	30.0
N2-N1-C5-H15	–	-179.9	180.0	–	–	-179.8	–	–
N2-N1-C5-H10	59.1	180.0	0.1	–	179.9	179.9	–	-180.0
System	TS3	**6**	**7**	TS4	**8**	**9**	TS5	**10**
Lengths (Å)								
N1-N2	1.316	–	1.350	1.318	–	1.351	1.319	–
N2-C3	2.124	–	1.488	2.172	–	1.490	2.209	–
C3-C4	1.407	1.331	1.538	1.412	1.335	1.538	1.417	1.339
C4-H15	1.352	–	1.090	1.332	–	1.093	1.305	–
N1-H15	1.333	–	–	1.355	–	–	1.385	–
C4-H13	1.089	1.086	1.093	1.088	1.085	1.090	1.092	1.089
N1-C5	1.346	–	1.330	1.347	–	1.331	1.347	–
N2-C7	1.343	–	1.361	1.342	–	1.361	1.343	–
Angles (º)								
N1-N2-C3	100.7	–	118.8	100.8	–	118.8	100.0	–
N2-C3-C4	97.9	–	108.2	96.3	–	107.8	96.2	–
N1-H15-C4	145.7	–	–	147.0	–	–	149.5	–
C3-C4-H15	96.8	–	110.4	97.9	–	110.6	96.7	–
N2-N1-H15	98.8	–	–	98.0	–	–	97.0	–
C3-N2-C7	150.5	–	129.7	150.5	–	129.6	151.3	–
N1-C5-H10	121.2	–	119.6	121.3	–	119.6	121.2	–
C3-C4-H13	117.0	121.7	110.7	116.9	121.6	110.7	113.4	116.9
Dihedral angles (º)								
N1-H15-C4-H13	123.7	–	–	120.1	–	–	125.9	–
N1-N2-C3-C4	2.3	–	-59.9	0.0	–	-55.9	5.3	–
N2-N1-C5-H15	175.3	–	–	0.0	–	–	179.5	–
N2-N1-C5-H10	180.0	–	180.0	180.0	–	179.7	180.0	–

(-0.582) in **1**. The observed trends closely parallel the theoretical findings reported by Elliott *et al*. [20] regarding alkyl group effects in organic molecules. Examination of reactions II and III revealed that substitution of methyl groups at the α-carbon (C3) and β-carbon (C4) positions in **4a**, as well as ethyl substitution at the α-carbon (C3) position in **4b**, exerted only a limited effect on the structural parameters. Despite the minor geometrical changes, distinct differences were observed in the energetic profiles of the reactions, which are discussed subsequently.

Formation of pyrazole and 2-methylpropene (reaction IV): In reaction IV, N-*tert*-butyl pyrazole (**7**) converts to 2-methylpropene (**8**) and pyrazole (**2**) *via* TS4. Various changes in structural parameters, *viz.* bond lengths, bond angles and dihedral angles are found to be similar to that in other three reactions (I, II and III) that are discussed earlier in the section.

TABLE-2
SOME SELECTED BONDING CHARACTERISTICS OF REACTION PATHS USING B3LYP/6-311++G(d,p) OPTIMISED GEOMETRY

System	N1- N2		N2- C3		N1-H15		C3-C4		C4-H15	
	$\rho(r_c)$ (e/au^3)	∇^2 ρ_c (e/au^5)	$\rho(r_c)$ (e/au^3)	$\nabla^2\rho_c$ (e/au^5)	$\rho(r_c)$ (e/au^3)	$\nabla^2\rho_c$ (e/au^5)	$\rho(r_c)$ (e/au^3)	$\nabla^2\rho_c$ (e/au^5)	$\rho(r_c)$ (e/au^3)	$\nabla^2\rho_c$ (e/au^5)
1	0.368	-0.682	0.257	-0.657	–	–	0.243	-0.555	0.276	-0.925
TS1	0.403	-0.842	0.076	0.093	0.162	-0.021	0.299	-0.799	0.122	-0.142
2	0.378	-0.690	–	–	0.344	-1.754	–	–	–	–
3	–	–	–	–	–	–	0.344	-1.029	–	–
4a	0.338	-0.417	0.234	-0.435	–	–	0.226	-0.394	0.260	-0.741
TS2	0.400	-0.824	0.059	0.094	0.136	-0.076	0.302	-0.811	0.148	-0.239
5	–	–	–	–	–	–	0.277	-0.934	–	–
4b	0.368	-0.681	0.251	-0.631	–	–	0.243	-0.553	0.276	-0.921
TS3	0.399	-0.820	0.059	0.093	0.141	-0.100	0.300	-0.807	0.143	-0.218
6	–	–	–	–	–	–	0.342	-1.015	–	–
7	0.368	-0.680	0.249	-0.611	–	–	0.240	-0.537	0.280	-0.918
TS4	0.398	-0.812	0.054	0.089	0.133	-0.068	0.299	-0.080	0.150	-0.246
8	–	–	–	–	–	–	0.341	-1.000	–	–
9	0.366	-0.670	0.243	-0.595	–	–	0.237	-0.518	0.274	-0.910
TS5	0.397	-0.807	0.050	0.087	0.124	-0.029	0.297	-0.790	0.161	-0.293
10	–	–	–	–	–	–	0.337	-0.969	–	–

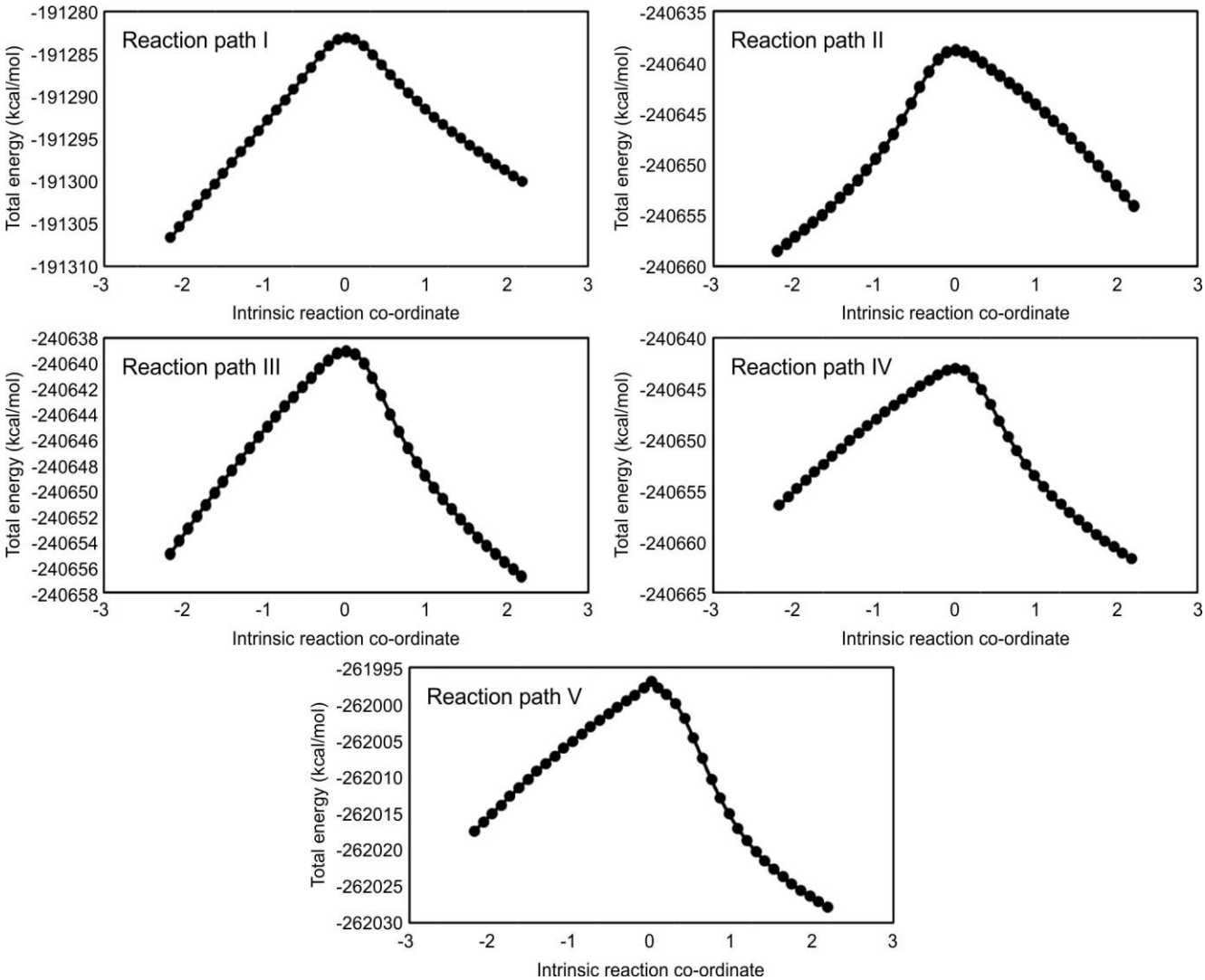

Fig. 3. Potential energy profile (PES) for reaction path I and Path II. Zero point presents the transition state along the IRC. The negative represents the reactant and products are towards positive directions

TABLE-3
CALCULATED HARMONIC VIBRATIONAL FREQUENCIES (cm^{-1})
(SCALED BY 0.9679) USING B3LYP/6-311G++(d,p) OPTIMISED GEOMETRY

1	**2**	**3**	**4a**	**4b**	**5**
726 (73)	507 (61)	943 (112)	727 (70)	727 (70)	966 (42)
1022 (20)	665 (21)	3021 (17)	1024 (24)	1024 (24)	1450 (22)
1074 (21)	727 (100)	3118 (25.6)	1382 (24)	1382 (24)	2913 (75)
1275 (21)	1012 (41)		1420 (28)	1420 (28)	2953 (47)
1380 (27)	1105 (24)			2926 (26)	2986 (20)
1495 (23)	3547 (88)			2939 (37)	
2937 (22)				2988 (36)	
2958 (24)				3002 (61)	
3003 (33)					

6	**7**	**8**	**9**	**10**
913 (51)	723 (68)	888 (52)	724 (68)	1445 (21)
2907 (26)	1065 (25)	1442 (19)	941.8 (21)	2906 (29)
2926 (33)	1206 (28)	1453 (16)	1064 (23)	2913 (85)
2986 (38)	1250 (41)	1656 (23)	1285 (22)	2949 (40)
2993 (35)	1300 (21)	2910 (21)	1378 (33)	2996 (20)
3011 (33)	1379 (30)	2916 (44)	2933 (30)	3015 (23)
	1491 (19)	2955 (46)	2990 (32)	3023 (57)
	2934 (15)	3002 (29)	2997 (24)	
	2935 (25)	3003 (20)	3001 (35)	
	3001 (34)		3006 (24)	
	3009 (50)		3018 (28)	

TS1	TS2	TS3	TS4	TS5
1334i (1523)	1187i (1402)	1243i (1630)	1171i (1720)	1033i (1455)
263 (236)	197.2 (56.4)	906 (27)	168 (96.5)	175 (69)
407 (72.3)	206.2 (21.3)	1030 (36)	307 (57.8)	323 (90)
753 (77.4)	334.4 (157)	1049 (24)	362 (60.2)	575 (90)
870 (27.2)	516.7 (27.8)	1069 (37)	418 (21.5)	744 75)
907 (20.7)	747.9 (76.7)	1224 (72)	550 (60)	750 (67)
1034 (59.8)	845 (26.4)	1307 (22)	747 (74.9)	819 (25)
1079 (39.4)	901.9 (21)	1320 (58)	1295 (61.9)	1015 (47)
1176 (72)	1013 (81.8)	1461 (21)	1342 (47.1)	1044 (54)
1209 (111)	1037 (45.4)	1489 (30)	1350 (26.8)	1074 (101)
1328 (65.5)	1031 (20)	1630 (48)	1361 (21.3)	1287 (67)
1450 (24.2)		2961 (27)	1486 (29.9)	1307 (38)
1487 (20.6)			1593 (46.9)	1411 (30)
1685 (84.1)			2917 (39.1)	1487 (43)
				1572 (36)
				2911 (41)

Figures in parentheses are the computed intensities (km/mol)

TABLE-4
NATURAL ATOMIC CHARGES

System	N1	N2	C3 (α)	C4 (β)	H15
1	-0.302	-0.217	-0.160	-0.582	0.216
TS1	-0.345	-0.255	-0.138	-0.720	0.379
2	-0.341	-0.295	–	–	0.401
3	–	–	-0.366	-0.366	–
4a	-0.307	-0.226	0.004	-0.389	0.214
TS2	-0.353	-0.285	0.075	-0.521	0.381
5	–	–	-0.185	-0.185	–
4b	-0.307	-0.226	0.004	-0.577	0.218
TS3	-0.353	-0.285	0.075	-0.702	0.373
6	–	–	-0.614	-0.385	–
7	-0.307	-0.231	0.146	-0.578	0.226
TS4	-0.359	-0.294	0.244	-0.702	0.374
8	–	–	-0.004	-0.401	–
9	-0.307	-0.231	0.156	-0.389	0.227
TS5	-0.360	-0.301	0.265	-0.524	0.381
10	–	–	-0.024	-0.196	–

Lengthening of N2-C3 and C4-H15 bond length and shortening of C3-C4 and N1-N2 bond length is observed (Table-1). Bond angles, N1-N2-C3, N2-C3-C4 and C3-C4-H15 decreases, which facilitates the formation of five-membered cyclic transition state TS4 along with N2-N1-H15 bond angle equal to 98°. Magnitude of $\rho(r_c)$ and $\nabla^2\rho_c$ also supports the changes observed in the bond lengths (Table-2). Only one negative frequency for the TS4 and all positive vibrational frequencies for the reactant (**7**) and product (**8**) suggests the acceptable TS and stable geometries of reactant and product (Table-3). Natural atomic charge on C3 atom (0.146) in **7** is large and positive as compared to the reactants, *viz.*, **1**, **4a** and **4b** which shows the effect of two methyl group substitution on C3. After comparing the charges on C3 atom among the aforementioned reactants, we can see that the methyl group has electron withdrawing effect. Furthermore, the C3 atom in TS4 is found to be more positive with charge equal to 0.244. The H15 atom moves to the N1 of the pyrazole ring as a proton

as we can see that the negative charge on C4 atom increases in TS4 from -0.578 to -0.702.

Formation of pyrazole and 2-methylbut-2-ene (reaction V): In reaction V, N-*tert*-pentyl pyrazole (**9**) converts to 2-methylbut-2-ene (**10**) and pyrazole (**2**) through TS5. The structural parameter variations presented in Table-1 exhibit trends comparable to those observed in the other four reactions (I-IV). The TS5 structure is valid as indicated by the single negative frequency with high magnitude and intensity and vibrational frequencies for the reactant **9** and product **10** are all positive suggesting the stable geometries of the two (Table-3). Natural atomic charge on C3 atom (0.156) in **9** is maximum as compared to all other considered reactants due to the effect of two methyl group on C3 and one methyl group on C4 atom. After comparing the charges among all the reactants, it has been observed that charge on C3 atom changes from negative (-0.160 in **1**) to positive (0.156 in **9**). This observation suggests the effect of substitution on C3 and C4 atom from all H's ($R_1 = R_2 = R_3 = H$) to all methyl ($R_1 = R_2 = R_3 = CH_3$). A negative inductive effect of the methyl group was observed in the present study. In addition, the C3 atom in TS5 showed the maximum positive charge of 0.265.

The structural parameters calculated for all five transition states, namely TS1, TS2, TS3, TS4 and TS5, exhibited closely related geometrical features, including bond lengths, bond angles and dihedral angles. The elongation of the N2–C3 and C4–H15 bonds during bond cleavage followed nearly identical trends in all five reaction pathways. In addition, the N1–H15 bond distances remained similar across the transition states. However, substituent changes at the C3 and C4 positions resulted in noticeable differences in the corresponding atomic charges.

Energetics of the reactions I to V: To understand the energetics of the β-elimination reaction of *N*-alkyl substituted pyrazoles, the thermodynamic analysis for all the five reactions is done at B3LYP level using 6-311++G(d,p) basis set and tabulated in Table-5. Amongst all the five reactions, E_a for the reaction I is maximum where, $R_1 = R_2 = R_3 = H$ and least for the reaction V where, $R_1 = R_2 = R_3 = CH_3$. All the reactions are found to be endothermic in nature. The ΔH values for the five considered reactions follow the order, I > III > II > IV > V. The obtained DFT results agree with the experimental kinetic study with respect to the trend in activation energies and reaction enthalpies, although the calculated values are lower in magnitude [10]. Compared with the experimental data, the DFT calculations underestimated the enthalpies of all the reactions. In contrast, semi-empirical calculations reported earlier predicted activation energies approximately 25 kcal mol^{-1} higher than the experimental values [11]. The relative energies of the reactants, transition states and products along the reaction coordinate are shown in Fig. 4. The entropy for all the five reactions was calculated and as expected for a dissociation reaction, there is a positive change in the value of ΔS. The free energy values are also calculated for the five reaction paths at 298.15 K. The ΔG values were found to be positive at this temperature for the reaction I to IV. For the reaction V, even at 298.15 K, ΔG values becomes negative due to the three methyl groups at C3 and C4 position. Thermolysis reactions in gas phase are usually carried out at high temperatures between 800 to 1300 K. At such high temperature, the TΔS term contributes significantly and ΔG becomes negative for the reaction. The calculations in this study were conducted at 298.15 K; therefore, consideration of higher temperatures is expected to produce negative Gibbs free energy values for all the investigated reactions.

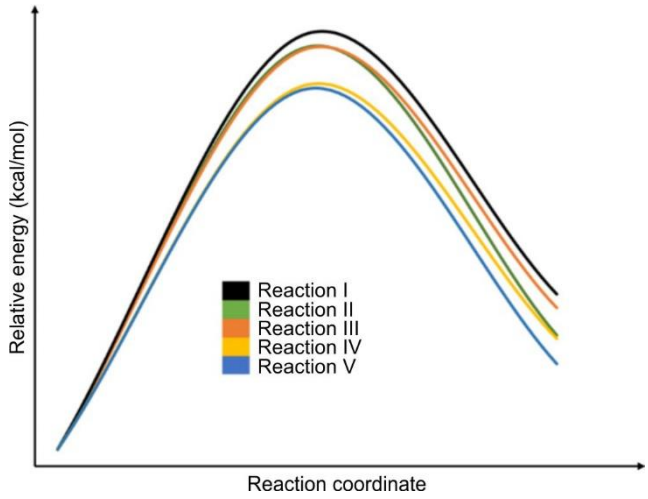

Fig. 4. Relative energy barrier comparison for the five reaction paths

Conclusion

The present DFT study investigates the β-elimination reactions of N-alkyl pyrazoles with five different substituent combinations at α- and β-carbon atom. Five reaction paths (I to V) are studied in detail using B3LYP/6-311G++(d,p) with substituents (R_1, R_2 and R_3) that are the combination of H, methyl and ethyl group. In the considered reactions (I to V) N-ethyl pyrazole, N-*sec*-butyl pyrazole (reaction II & III), N-*tert*-butyl pyrazole and N-*tert*-pentyl pyrazole converted to ethene, but-2-ene, but-1-ene, 2-methylpropene and 2-methyl-but-2-ene, respectively with pyrazole as the common product

TABLE-5
CALCULATED ENTROPY (ΔS) (kcal mol^{-1}), ACTIVATION ENERGIES (E_a), ENTHALPY (ΔH) AND FREE ENERGY (ΔG) OF REACTIONS (kcal mol^{-1}) USING B3LYP/6-311++G(d,p)

Reaction	ΔS	Activation energy (E_a)		ΔH		ΔG
Reaction I	36.3	49.7	(56.0)[a]	18.6	(24.2)[a]	7.7
Reaction II	41.1	48.0	(54.2)[a]	13.6	(24.1)[a]	1.4
Reaction III	42.2	47.9		16.9		4.3
Reaction IV	42.5	43.5	(53.0)[a]	13.2	(24.9)[a]	0.6
Reaction V	45.1	43.1		10.2		-3.2

[a]Experimental value taken from reference [10]

in all the reaction paths. All the five reactions are endothermic in nature. An acceptable planar five membered transition state formed in the reactions as only one imaginary frequency with high intensity is observed for all the five TS's. The H attached to β-C atom moves to N of pyrazole ring as a proton as charge on β-C atom becomes more negative in TS. Substitution with methyl groups at α- and β-C atom, *i.e.*, $R_1 = R_2 = R_3 = CH_3$ decreases the activation energy as well as enthalpy of the reaction when compared to other four reactions. Furthermore, on comparing the charge on C3 and C4 atom among all the reactants, present study suggests that methyl and ethyl group have negative inductive effect on these two α- and β-C atoms that is also in concordance with a recent theoretical study. The energetic trends obtained in this study are in close agreement with the previously reported experimental kinetic results and are more accurate than those predicted by earlier semi-empirical calculations. The present investigation contributes to a deeper theoretical understanding of substituent effects in the β-elimination reactions of *N*-alkyl pyrazoles.

ACKNOWLEDGEMENTS

The authors are grateful to University of Delhi and Zakir Husain Delhi College for providing the necessary resources to carry out the present work.

CONFLICT OF INTEREST

The authors declare that there is no conflict of interests regarding the publication of this article.

DECLARATION OF AI-ASSISTED TECHNOLOGIES

During the preparation of this manuscript, the authors used an AI-assisted tool(s) to improve the language. The authors reviewed and edited the content and take full responsibility for the published work.

REFERENCES

1. R.I.L. Meador, N.A. Mate and J.D. Chisholm, *Organics*, **3**, 111 (2022); https://doi.org/10.3390/org3020009
2. J.V. Faria, P.F. Vegi, A.G.C. Miguita, M.S. dos Santos, N. Boechat and A.M.R. Bernardino, *Bioorg. Med. Chem.*, **25**, 5891 (2017); https://doi.org/10.1016/j.bmc.2017.09.035
3. M.-C. Ríos and J. Portilla, *Chemistry*, **4**, 940 (2022); https://doi.org/10.3390/chemistry4030065
4. Y. Li, F.A. Lakhvich, T.S. Khlebnicova, Y. Fu and F. Ye, *J. Agric. Food Chem.*, **73**, 24528 (2025); https://doi.org/10.1021/acs.jafc.5c08390
5. M. El Boutaybi, A. Taleb, R. Touzani and Z. Bahari, *Mater. Today Proc.*, **31**, S96 (2020); https://doi.org/10.1016/j.matpr.2020.06.249
6. Y.Q. Gu, W.Y. Shen, Y. Zhou, S.F. Chen, Y. Mi, B.F. Long, D.J. Young and F.L. Hu, *Spectrochim. Acta A Mol. Biomol. Spectrosc.*, **209**, 141 (2019); https://doi.org/10.1016/j.saa.2018.10.030
7. A. Tigreros and J. Portilla, *RSC Adv.*, **10**, 19693 (2020); https://doi.org/10.1039/D0RA02394A
8. S. Zhang, Z. Gao, D. Lan, Q. Jia, N. Liu, J. Zhang and K. Kou, *Molecules*, **25**, 3475 (2020); https://doi.org/10.3390/molecules25153475
9. G.I. Yranzo and E.L. Moyano, *Curr. Org. Chem.*, **8**, 1071 (2004); https://doi.org/10.2174/1385272043370113
10. J.D. Perez and L.M. Phagouape, *Int. J. Chem. Kinet.*, **19**, 571 (1987); https://doi.org/10.1002/kin.550190608
11. J.D. Perez, L.M. Phagouapé and G.E. Davico, *J. Phys. Org. Chem.*, **2**, 225 (1989); https://doi.org/10.1002/poc.610020305
12. A.D. Becke, *Phys. Rev. A*, **38**, 3098 (1988); https://doi.org/10.1103/PhysRevA.38.3098
13. A.D. Becke, *J. Chem. Phys.*, **98**, 5648 (1993); https://doi.org/10.1063/1.464913
14. C. Lee, W. Yang and R.G. Parr, *Phys. Rev. B Condens. Matter*, **37**, 785 (1988); https://doi.org/10.1103/PhysRevB.37.785
15. R.F.W. Bader, *Acc. Chem. Res.*, **18**, 9 (1985); https://doi.org/10.1021/ar00109a003
16. M.P. Andersson and P. Uvdal, *J. Phys. Chem. A*, **109**, 2937 (2005); https://doi.org/10.1021/jp045733a
17. R.G. Parr and W. Yang, Density Functional theory of Atoms and Molecules, Oxford University Press: New York, Oxford, pp. IX+333 (1989).
18. J.K. Labanoeski and J.W. Andzelin, Density Functional Methods in Chemistry, Springer Verlag: New York (1991).
19. S.H. Vosko, L. Wilk and M. Nusair, *Can. J. Phys.*, **58**, 1200 (1980); https://doi.org/10.1139/p80-159
20. M.C. Elliott, C.E. Hughes, P.J. Knowles and B.D. Ward, *Org. Biomol. Chem.*, **23**, 352 (2025); https://doi.org/10.1039/D4OB01572J